Investigation of europium retention on Callovo-Oxfordian clay rock (France) by laser ablation inductively coupled plasma mass spectrometry (LA-ICP-MS) and percolation experiments in microcells

Y. Hassan Loni, K. David, S. Ribet, Philippe Lach, Catherine Lerouge, B. Madé, C. Bailly, B. Grambow, Gilles F Montavon

Investigation of Europium Retention on Callovo-Oxfordian Clay Rock (France) by Laser Ablation Inductively Coupled Plasma Mass Spectrometry (LA-ICP-MS) and percolation experiments in microcells.

Y. HASSAN LONI[1], K. DAVID[1], S. RIBET[1], P. LACH[2], C. LEROUGE[2], B. MADÉ[3], C. BAILLY[1], B. GRAMBOW[1] and G. MONTAVON[1]*

[1] Laboratoire SUBATECH, UMR 6457, IN2P3/CNRS/IMT Atlantique/Université de Nantes, 4, rue Alfred Kastler, BP 20722, 44307 Nantes cedex 3, France

[2] BRGM, 3 avenue Claude Guillemin, F-45060 Orléans, France

[3] Agence Nationale pour la gestion des Déchets Radioactifs (Andra), Direction Recherche & Développement, 1/7 Rue Jean Monnet, 92298, Châtenay-Malabry Cedex, France

*Corresponding author: montavon@subatech.in2p3.fr

Phone: +33 251 85 84 20

Abstract

Clay-rock formations are under investigation in several countries as a potential host of radioactive waste repositories. In order to assess the long-term safety of these concepts, retention distribution data (Rd) are needed to describe the interaction between radionuclides and natural rock. While Rd values obtained from batch-type experiments with dispersed material are essential for the development of retention models, it is also important to generate retention data under more realistic conditions, in particular with compact samples. Specifically, the literature data on strongly retained radionuclides proves to be very scarce. The present study

focuses on the retention of europium at trace concentrations on clay samples extracted from the Callovo-Oxfordian (COx) formation in France. Rd values obtained with compact COx samples are assessed by a methodology coupling percolation experiments (in pressurized microcells), performed using submillimeter-sized samples in thickness, and Laser Ablation Inductively Coupled Plasma Mass Spectrometry measurements. The Rd found at trace concentrations under non-transient conditions are high ($Rd > 10^4$ mL g^{-1}) and in agreement with those recorded under classical batch-type conditions or those deduced from the distribution of naturally-occurring Eu between the pore water and the clay rock. They can be described by modeling with existing sorption databases, considering an adsorption process only on the clay fraction. This was validated by solid state LA-ICP-MS analyses of one of the Eu-spiked COx samples; the added europium was found exclusively in the COx clay fraction.

Keywords: Retention, Clay rock, Europium, (LA)-ICP-MS, Percolation.

I. Introduction

The development of nuclear energy requires safe solutions for managing radioactive waste. The worldwide consensus on the best way to protect human life and the environment is to dispose of this radioactive waste in deep geological repositories. In France, the Callovo-Oxfordian claystone formation (COx) is under investigation as a geological barrier to lower the fluxes from the waste towards the geosphere, the hydrosphere and biosphere (ANDRA, 2005a; Sellin and Leupin, 2013). This clay-rich formation, located in the Meuse/Haute-Marne site (Eastern France), is characterized by low permeability, mineralogical homogeneity, high retention capacities for radionuclides and little variation in other physicochemical properties (ANDRA, 2005b; Grambow, 2016).

To assess the long-term safety of this repository site, it is important to understand, characterize and quantify the retention and transport properties of radionuclides in the host clay rock. Retention processes, such as adsorption on mineral surfaces, precipitation as poorly soluble pure solid phases, co-precipitation in the formation of minerals (neo-formation of a solid solution) or incorporation into solid phases, can delay the radionuclides migration (Maes et al., 2008) for a sufficient time to allow for radioactive decay.

"Safety analyses" generally consider adsorption processes (typically described by a list of retention distribution data, or Rd values) leading to retardation of mass transfer. Scientifically, for clayey rocks, these Rd values can be understood by cation exchange and surface complexation reaction describing the concentration of labile species in rapid equilibrium with a surface and a solution as a function of a number of environmental variables such as pH, pCO_2, ionic strength, etc. The formation of these labile species can be described by thermodynamic approaches. The modeling of radionuclide adsorption processes in the clay formation requires numerous input parameters, many of which have been determined under laboratory conditions with pure clay minerals. Experiments are carried out in batch-type mode in a state where the solid is dispersed in large quantities of synthetic pore water for reasons of either duration or ease of experimental implementation. The experiments are quite simple, relatively fast (a few days) and able to be performed under a variety of well-controlled conditions; also, the data can be used for assessing the dependency of retention parameters on the local mineralogy of the host rock and its variation, on temperature, or on parameters describing the pore water chemistry such as pH, pCO_2, redox, other chemical species as aqueous silica or salinity variations. However, it is essential to ensure that the adsorption parameters obtained on dispersed materials are capable of describing adsorption processes on the actual compact rock/pore water systems.

A relatively recent review (Miller and Wang, 2012) on the subject highlights various aspects that can lead to differences depending on the state of compactness of the sample (surface-water reactivity, accessibility of sorption sites, electrostatic considerations, double-layer overlapping, etc.). For the case of Cs, Van Loon and Glaus (2008) critically examined the application of thermodynamic models on highly compacted states whose ion hydration energies may differ from those in the dispersed state. This important subject must therefore be treated for each class of key radionuclides, which entails developing methods capable of determining retention parameters for compact states.

In the ideal case, it would be possible to carry out batch-type retention experiments in a compact system, i.e. waiting until a non-transient state is reached when the radionuclide concentration in aqueous solution (in contact with the water-saturated porous system) and the radionuclide concentration in pore water are equal. Under these conditions, the concentrations of radionuclides both in pore water and retained on the solid surface can be measured, which serves to calculate the distribution coefficient describing the retention (Rd) value. However, achieving a non-transient state can take a long time due to the low permeability of the studied compact clay materials. This approach appears to be feasible for highly compact states with poorly or moderately retained radionuclides. A few number of studies can be found in the literature for: I^- (Montavon et al., 2014), Cs^+ (André et al., 2009; Chen et al., 2014b; Oscarson, 1994; Van Loon et al., 2009), Ni^{2+} (Montavon et al., 2020), and Sr^{2+} (Van Loon et al., 2005). Overall, no clear evidence suggests that increasing clay compaction will lead to a fundamentally different uptake of radionuclides.

For strongly sorbed ions/radionuclides, like trivalent metal ions, retention data are often deduced from in-diffusion experiments, where information is derived from a transient state (Descostes et al., 2017; Glaus et al., 2020; Kasar et al., 2016; Wang et al., 2004). The information on metal retention is reliable provided species mobility has been adequately

described since compaction potentially affects both diffusive mass transfer and retention. Therefore, it is fundamental to develop for strongly sorbed elements, in parallel with transport/diffusion experiments, a set of methodologies yielding retention data in a non-transient state (i.e. concentrations of radionuclides both in pore water and retained on the solid surface can be measured), in order to assess the compaction effect on retention processes.

The objective of this work is to propose a non-transient method adapted to the retention study of strongly sorbed elements on compact clay rock samples. It combines the use of pressurized PEEK (Polyetheretherketone) micro cells, thereby limiting adsorption phenomena (Aertsens et al., 2003) and accommodating submillimeter-thick samples, with a percolation mode to accelerate transport so as to overcome the disadvantages of a long experimental duration by using diffusion cells (Montavon et al., 2020 ; Chen et al., 2014b). After the experiment, the strongly sorbed element is analyzed quantitatively on the (inlet) surface and in depth of the compact sample by means of Laser Ablation Inductively Coupled Plasma Mass Spectrometry (LA-ICP-MS). This technique turns out to be essential in the present context (due to its high sensitivity and spatial resolution) to determining metal ion concentration in metal-spiked compact samples as well as to assessing its distribution among the various mineral phases present in the clay rock.

The methodology adopted in this study is applied to the Eu/COx system. Indeed, Eu is considered to be a chemical homologue of certain trivalent actinides, such as Am or Cm, present in radioactive waste (Kautenburger and Beck, 2010). Europium retention values published in the literature are high and range from 5×10^4 to 10^5 L kg^{-1} for trace concentrations, thus reflecting a strong interaction with COx clay rock (ANDRA, 2005a; Descostes et al., 2017; Schott et al., 2012). Retention data obtained in the compact state are compared herein with data measured in the dispersed state and then discussed in light of both modeling results and a study of naturally-occurring Eu in COx clay rock.

II. Materials and methods

A summary of the experiments carried out in the present study is given in Table 1.

Two types of experiments were performed as part of this study, namely: batch-type sorption experiments on crushed COx samples in a dispersed state, and percolation experiments with compact clay rock. All experiments were conducted at T = 22 ± 2°C in the presence of a synthetic pore water (SPW) whose simplified composition was based on geochemical modeling exercises on *in situ* samples (Vinsot et al., 2008; Gaucher et al., 2009): $[Na^+] = 4.6\times10^{-2}$ M, $[K^+] = 10^{-3}$ M, $[Ca^{2+}] = 7.4\times10^{-3}$ M, $[Mg^{2+}] = 6.7\times10^{-3}$ M, $[Sr^{2+}] = 2\times10^{-4}$ M, $[Cl^-] = 4.1\times10^{-2}$ M, $[SO_4^{2-}] = 1.6\times10^{-2}$ M, inorganic carbon = 4.5×10^{-3} M (in equilibrium with calcite), and pH = 7.3. Inorganic carbon was controlled by use a N_2/CO_2 (1%) gas mixture ($P_{CO2} = 10^{-2}$ atm) either in a glove box (batch-type experiments) or by bubbling inlet solution (percolation experiments).

All solutions were prepared with ultra-pure deionized water (18.2 MΩ.cm) and with commercially available chemical products of analytical grade or superior. For the SPW preparation, analytical grade ≥99% ACS reagents (NaCl, Na_2SO_4 $10H_2O$, $CaCl_2$ $2H_2O$, $MgCl_2$ $6H_2O$, $NaHCO_3$, KCl) and $SrCl_2\cdot6H_2O$ product from Sigma Aldrich (99.995% trace metals basis) were used.

A stock solution of $EuCl_3$ (99.99% trace metals basis, Sigma Aldrich) was used to obtain initial concentrations of Eu between 1.9×10^{-9} and 1×10^{-7} mol L^{-1}. Sources of ^{152}Eu (Eckert & Ziegler) in 0.5M HCl (with 10µg/g of carrier) and HTO (Eckert & Ziegler) served as radioactive tracers.

II.1 COx samples

146 The COx samples used were obtained from the Meuse/Haute-Marne Underground Laboratory
147 (depth: ≈ 500 m) located in the eastern part of the Paris basin. They originated from boreholes
148 drilled by Andra (French Radioactive Waste Management Agency). The mineralogical
149 composition and proportions of the major phases have been extensively described in Gaucher
150 et al. (2004), ANDRA (2005b) and Lerouge et al. (2011). This composition mainly consists of
151 phyllosilicates (40-60 wt%, mainly illite and mixed layer illite/smectite, kaolinite and chlorite),
152 carbonates (15-45 wt%, mainly calcite and dolomite), tectosilicates (10-40 wt%, mainly quartz
153 and feldspars) and minority phases such as sulfides (0-3 wt%, mainly pyrite) and natural organic
154 matter (0.5-1 wt%).

155 After drilling, the samples were conditioned in airtight aluminum foil filled with nitrogen,
156 transported to the laboratory and then stored until their opening in a N_2/CO_2 (1%) glove box.

157 For the measurement of natural Eu concentrations in the pore water of COx, seepage water from
158 the Callovo-Oxfordian clay-rich rock was collected from borehole GIS1002 in Andra's
159 Meuse/Haute-Marne underground research laboratory. This 16-m long horizontal borehole was
160 drilled at a depth of 490 m in the clay-rich layer. The water sample analyzed was collected 10
161 years after the borehole began to produce water (Grangeon et al., 2015).

162
163 **II.2 Batch-type experiments**

164 Europium retention on COx was investigated by means of batch-type experiments as a function
165 of Eu concentration at a fixed solid/liquid (S/L) ratio (0.5 g L^{-1}). An appropriate amount of COx
166 powder (grain size < 200 µm) was dispersed in SPW in 35-mL Nalgene® Polypropylene
167 Copolymer (PPCO) centrifugation tubes. After one day of mechanical agitation to equilibrate
168 the "SPW/COx/atmosphere" system, Eu was added to the suspension. The Eu concentration
169 domain was chosen (by modeling) so as to avoid any precipitation of Eu hydroxide or carbonate
170 solid phases (see Table 1). Preliminary experiments showed that a contact time of at least 4

171 days was necessary to reach sorption equilibrium, as indicated by constant Eu concentrations
172 in the aqueous phase, within the uncertainties, as a function of the time (data not shown). The
173 supernatant was recovered using 0.22-µm surfactant-free cellulose acetate filters for Eu
174 analysis.

175 The solid/liquid distribution coefficient, Rd (in L kg^{-1}), and associated error (Err_{R_d}) were
176 determined according to the following equations:

177 $$\mathrm{Rd} = \frac{C_s}{C_{eq}} = \frac{C_0 - C_{eq}}{C_{eq}} \times \frac{V}{m} \quad (1)$$

178 where C_s (mol g^{-1}), C_0 (mol L^{-1}), C_{eq} (mol L^{-1}), V (L) and m (kg) are respectively: the amount
179 of Eu adsorbed onto the solid, the initial and equilibrium aqueous concentrations of Eu, the
180 volume of the aqueous solution, and the mass of the COx powder.

181 the associated error is calculated according to the equation:

182 $$Err_{R_d} = \sqrt{\left(\frac{V}{m}\frac{C_0}{C_{eq}}\right)^2 \times \left(\left(\frac{Err_{C_0}}{C_0}\right)^2 + \left(\frac{Err_{C_{eq}}}{C_{eq}}\right)^2\right) + {R_d}^2 \times \left(\frac{Err_{V/m}}{V/m}\right)^2} \quad (2)$$

183 with Err_{C0}, Err_{Ceq} and $Err_{V/m}$ being the uncertainties linked to C_0, C_{eq} and V/m, respectively.
184 In parallel to the sorption experiments, "blanks" were systematically performed with SPW in
185 the presence of Eu without COx to quantify the total Eu content (C_0); no significant adsorption
186 of Eu on either the tube surfaces or the filters under the experimental conditions of this study
187 was observed (<5%).

188 Each point on the isotherm corresponds to the result of a single test.

189 **II.3 Percolation experiments**

190 *II.3.1 Experimental strategy*

191 The methodology applied for percolation experiments involves injecting the element of interest
192 (at a given concentration) under pressure through the compact clay medium saturated with
193 synthetic pore water (in equilibrium with the phases present) (see Table 1 for more details).
194 We recall that the objective is to obtain a non- transient state, i.e. that element concentration at
195 the output of the assembly is equal to the injected concentration. Since the solution
196 concentration is known, a value for Rd can be calculated by determining the concentration of
197 the element in the adsorbent phase, here COx. It is also worth mentioning here that the transient
198 /non- transient state is not related to the notion of the establishment of an equilibrium state
199 between the soluble and adsorbed fractions of the element. This equilibrium state, which allows
200 the application of thermodynamic models, is dependent on the rate of adsorption of the element
201 onto the material. Such a state of equilibrium for the adsorption process is assumed with clays,
202 whether we are working under transient or non-transient conditions.
203 If we come back to our percolation experiences, a non-transient state can be obtained for
204 Cs/COx (Chen et al., 2014b) or Ni/COx (Montavon et al., 2020) systems. For the case of Eu,
205 which is a strongly retained element, this condition is more complicated to achieve. By way of
206 illustration, Fig. 1 shows initial simulations that were carried out with literature data, i.e. a value
207 of Rd around 10^5 L kg^{-1} (ANDRA, 2005a; Descostes et al., 2017; Schott et al., 2012). It can be
208 seen that the non-transient state is reached after about 6 years of experiments, even though the
209 work is being carried out in advective mode with submillimeter-sized samples in thickness (Fig.
210 1).

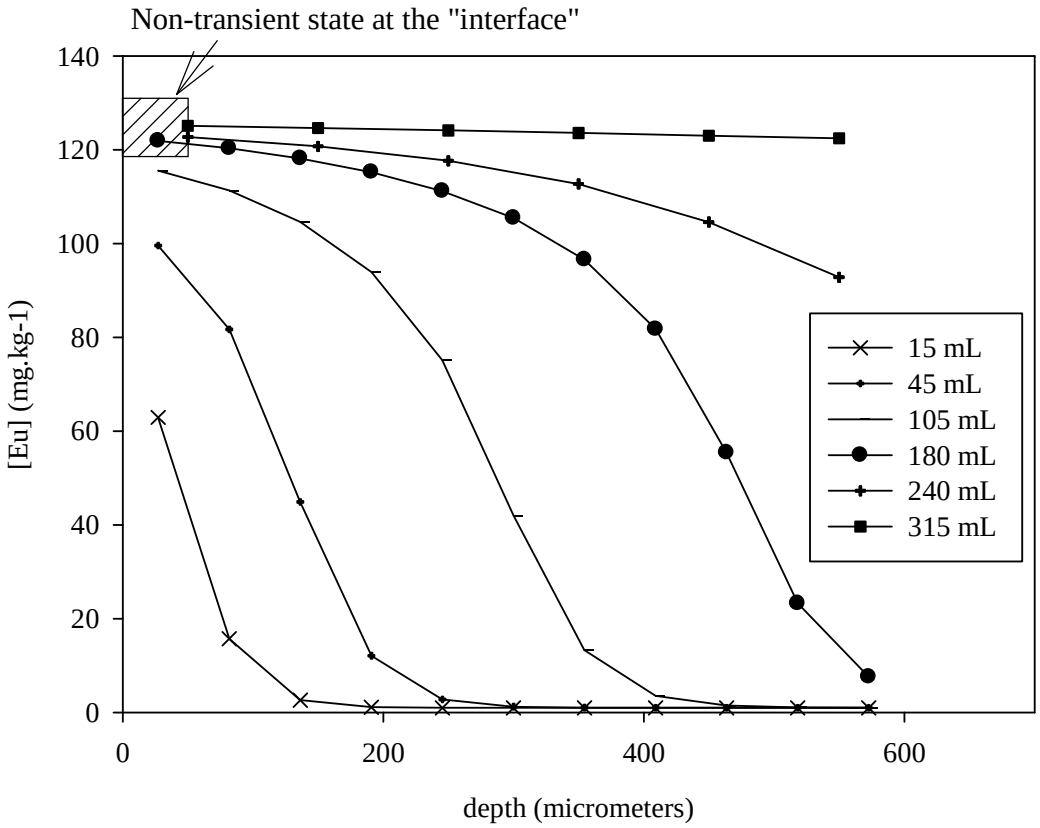

Fig.1: Simulations of Eu profile evolution in a compact COx sample vs. depth for different percolation volumes (for roughly 6 years of experiment). Flow rate: 0.15 mL day^{-1}; sample thickness: 0.6 mm; $[Eu]_{injected}=8.2\times10^{-8}$ M; $Rd=7.8\times10^{4}$ L kg^{-1}. Information for the simulation is available in Table A1.

In order to limit the experimental time (i.e. a few months), the strategy adopted in our study sought a non-transient state at the inlet surface, or at least within the first few micrometers. By measuring Eu concentration at the surface by LA-ICP-MS ($[Eu]_{clay,COx}$, in mol per mass of COx) with a known Eu concentration in the injection loop ($[Eu]_{injected}$, in mol per volume of SPW) it is then be possible to calculate a Rd value:

$$Rd = \frac{[Eu]_{clay,COx}}{[Eu]_{injected}} \quad (3)$$

The amount of spiked Eu in the COx was systematically corrected from the amount of Eu naturally present.

The retention parameter obtained can subsequently be used as a fixed value in an attempt to reproduce the Eu “percolation depth profiles” using a reactive transport model (see part II.5).

II.3.2 COx clay rock samples

Naturally highly compact samples were used (bulk density of ~2.3 g cm^{-3}). The sample preparation methodology was adapted from Montavon et al. (2020, 2014). First, a 1-cm diameter piece (several centimeters long) was manufactured through core drilling; next, a lathe (Caseneuve HB55) was used to obtain a diameter of 4.99 ± 0.02 mm. Lastly, the piece was fastened onto a support and cut into slices (thickness: 0.5 - 0.8 ± 0.05 mm) by means of a precision diamond wire saw (Escil® W3032; wire diameter = 0.3 mm). These steps were performed under air, but the potential superficial oxidation of the minerals was minimized by using a nitrogen flow around the rock samples. Note that a possible partial oxidation of the sample will not have a direct effect on the retention of Eu: Eu is not a redox sensitive element and neither is the clay fraction of COx.

The dry bulk densities of the pellets output ranged from 2.18 to 2.28 g cm^{-3}.

The samples were initially qualitatively characterized by Optical Microscopy (Olympus BH2) and Scanning Electron Microscopy (Tescan Mira 3 XMU) (SEM) in order to select the "right candidates" (Fig. A1). The aim of this initial characterization was to discard COx pellets with cracks or those with crumbled edges and then select only those pellets characterized by a homogeneous distribution of COx mineral phases (compared to average compositions).

II.3.3 Percolation experiment set-up

The percolation experiment set-up is presented in Figure 2. The reactors have been designed to ensure total system tightness and allow for total sample recovery once the experiment has been completed. The material used to make the reactors and the capillary tubes are made of PEEK

in order to avoid or limit Eu adsorption phenomena (Molera and Eriksen, 2002). An assembly of three reactors R1, R2 and R3 connected in parallel was installed for the purpose of performing several experiments with just a single pump. Each part of the percolation cell was cleaned successively with HNO_3 5% (v/v), Milli-Q water and Normapur 96% ethanol before drying (in the glove box) and use.

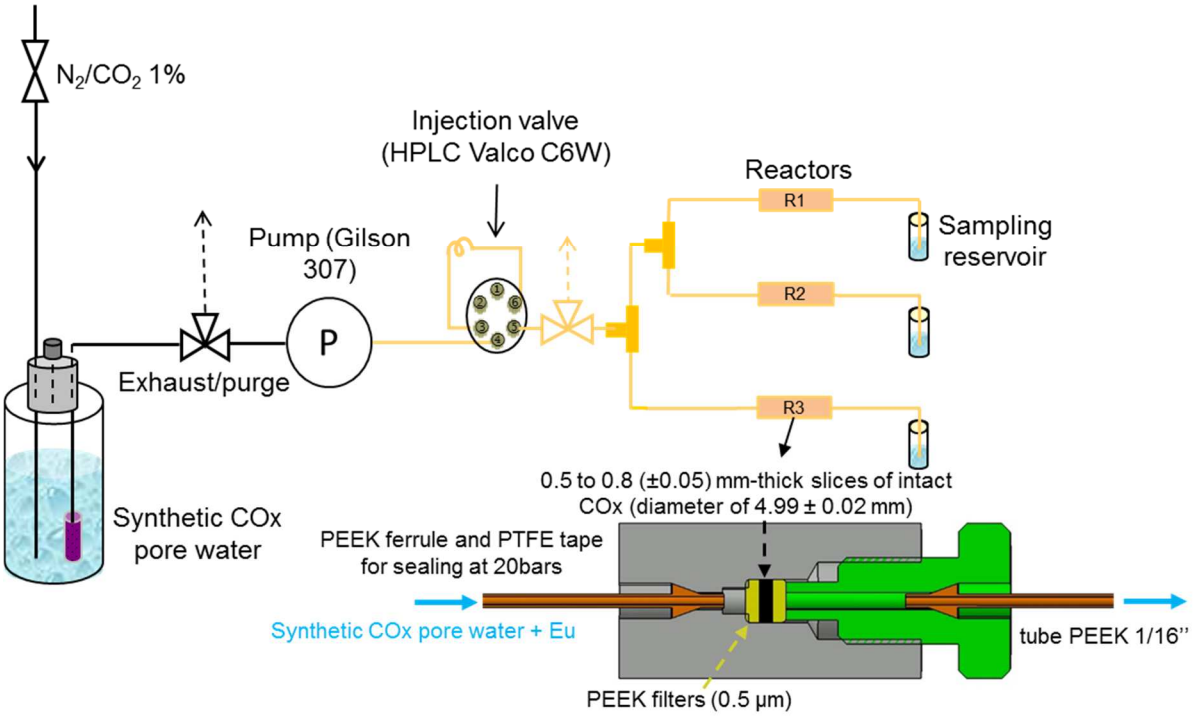

Fig. 2: The percolation experiment set-up

Once the samples had been inserted into the cells (between two PEEK filters), they were first hydrated and equilibrated with SPW. Sample hydration proceeded in stages, initially at low pressure (1 bar) for 3 days before pressure was gradually increased to 20 bar so as to determine the permeability and verify the applicability of Darcy's Law (Fig. A2). Average flows were 158 ± 10, 132 ± 7 and 101 ± 9 mg d^{-1} for R1, R2 and R3, respectively. In order to maintain the pH and carbonate concentration of the SPW constant throughout the duration of the experiment, a bubbling with a N_2/CO_2 (1%) gas mixture was carried out for at least 15 min twice a week. In the meantime, pH was measured from time to time in the sampling reservoir to ensure that the

system remained in equilibrium. SPW with Eu at $(8.8 \pm 0.9)\times10^{-8}$ mol L^{-1} was injected into the percolation cell at a constant pressure of 20 bar. In order to avoid Eu adsorption on the pump head, the solution was injected via a 7.85 mL injection loop (made of PEEK) (Fig. 2). In other words, the Eu-free SPW solution in the vessel in Fig. 2 "pushes" the Eu-doped SPW solution (present in the loop) into the compacted COx pellet. Note that the loops were changed in time to ensure a constant supply in Eu concentration in the COx. The outlet solution was analyzed regularly to both control the possible presence of Eu and measure pH values and alkalinity.

Europium solution percolation through samples R1, R2 and R3 was stopped after 174, 365 and 694 days, respectively. The collected solution volumes were of 25, 49 and 58 mL for R1, R2 and R3, respectively. Compact COx samples extracted from R1 and R2 reactors were recovered and cut in half using a sterilized scalpel (washed in AnalaR Normapur® 96% vol. ethanol (VWR BDH Prolabo) and 5% (v/v) Teflon distilled nitric acid and then rinsed with Milli-Q water).

The Eu "percolation depth profiles" were obtained by analyzing the side of the pellet in depth (from the surface in contact with the input solution to the end of the pellet from which the solution was recovered).

Each half-sample piece was fastened onto a thin petrographic plate with a double-sided adhesive disc for the Eu microanalysis of sample surface and depth profile by means of Laser Ablation Inductively Coupled Plasma Mass Spectrometry. For R1 and R2 samples, Eu concentrations were measured in relation to the mass of COx ablated. For R3, the analysis was concentrated on the clay fraction of the COx.

Results were compared with the distribution of Eu naturally present.

Table 1: Summary of the experimental conditions in effect during this study

Sample	Type of sample	Type of experiment	Focus	Contact time (days)	Figure(s)
EST45989 (R1)	Compact	Spiked by percolation	Eu concentration at the surf*ace and as a function of depth. $[Eu]_{injected}$ = (2.4 - 2.7)×10^{-8} mol L^{-1*}	174	5, 6, A1-2, 5
EST45989 (R2)				365	5, 6, A1-2, 5
EST45989 (R3)			Eu in clay fraction at the surface. $[Eu]_{injected}$ = 9.1×10^{-8} mol L^{-1*}	694	5, A1-2, A6
EST51779	Crushed	Spiked in the dispersed state	Rd measurement: $[Eu]_0$ = 1.9×10^{-9}-10^{-6} mol L^{-1} (experiments with the radioactive tracer)	4	3
EST51779	Compact	Naturally-occurring Eu	Eu distribution in COx mineral phases	-	3, 4, A1, A3

* concentrations measured at the end of the experiment; the initial concentration injected was (8.8 ± 0.9)×10^{-8} mol L^{-1}

II.4 Analytical techniques

The SPW composition was measured by ionic chromatography (Dionex ICS1000). A pH electrode (Inlab), freshly calibrated with standard pH buffers (pH 4, 7 and 10, Fisher), was used to measure pH values. The alkalinity was determined by colorimetric analysis using Bromocresol Green-Methyl Red Indicator Powder Pillow as color indicator and a Digital Titrator (Hach method 8203) with a digital titrator cartridges containing 0.16 N of H_2SO_4. Analyses of radioactive Eu (^{152}Eu) in solution (8 mL) were performed by liquid scintillation counting with a Packard TriCarb 3170 TR in adding an Ultima Gold LLT® (Perkin Elmer) scintillation cocktail (12 mL).

Direct analyses of Eu concentration in COx samples were conducted by LA-ICP-MS on thin samples polished under dry conditions in order to avoid any contamination or loss of trace element with reagents. Analyses of both natural (surface Eu concentration) and compact spiked COx R1 and R2 (depth profile and surface Eu concentration) samples were measured by LA-HR-ICP-MS at the SUBATECH Laboratory. Analyses of Eu concentration in the clay fraction of the compact Eu-spiked COx sample from the R3 reactor were performed by LA-Q (quadrupole)-ICP-MS at the BRGM (French Geological Survey) facility.

In order to identify the phases at the origin of Eu retention (Eu-COx sample from R3, natural COx sample), mineral phases (pyrite, calcite and clay fractions) were first characterized using an Olympus BH2 optical microscope (Fig. A3) and then localized by diamond strapping to assist with the analyses.

Note that the ability of the LA-ICP-MS technique to accurately quantify the amount of Eu was assessed with the natural sample by comparison with the amount measured in solution after sample acid digestion (Fig. A6).

II.4.1 LA-HR-ICP-MS

Micro-analyses of Eu in the natural COx or Eu-spiked COx (R1 and R2) samples were undertaken using a Nd-YAG UP213 laser system (NewWave Research) coupled with the Element XR single collector high resolution ICP-MS (Thermo Scientific). The HR-ICP-MS was synchronized to the laser ablation device in external trigger mode. The laser system was equipped with a standard ablation cell (V=30 ml) mounted on a motorized xyz stage with sub-micron resolution for sample movement. The ablated material was removed from the sample chamber by helium carrier gas, then mixed with argon gas and directly introduced into the hot plasma of the HR-ICP-MS instrument. Operating conditions have been detailed elsewhere (Hassan Loni et al., 2019). The Eu concentration was determined by external calibration using two standard reference materials, i.e. the NIST 610 synthetic glass with [Eu] (mg kg^{-1}) = 447 ± 10 (k=2) and the matrix-matched NIST 679 brick clay with [Eu] (mg kg^{-1}) = 1.9 ± 0.2 (k=2) prepared in a compacted disc-shaped pellet. The quantification procedure was carried out according to two distinct approaches, namely: internal standardization with a major element of known concentration used as internal standard, and the 100% oxide normalization in applying the total matrix (58 elements) as an internal standard (Lin et al., 2016; Liu et al., 2008; Šelih and Van Elteren, 2011; Van Elteren et al., 2009).

The Eu depth profiles of R1 and R2 COx samples were analyzed in either line scan or single-spot ablation modes according to the 100% oxide (w/w) normalization strategy. The laser was operated at a pulse repetition rate of 10 Hz, with an output energy of 50% (≈ 0.5 mJ) and beam diameter of 65 µm (line scan) or 50 µm (single spot). A total analysis time of 3 min was defined for the line ablation mode (2 min for the single-spot mode), including 2.25 min (or 1 min) and 1.7 min (or 1 min) for laser ablation sample and gas blank measurements, respectively.

Micro-analyses of Eu in polished thin sections of natural COx mineral phases were performed by both external calibration and internal standardization (^{29}Si or ^{27}Al for clay fraction, ^{42}Ca for calcite and ^{57}Fe for pyrite). The laser settings were as follows: output energy = 50% (≈ 0.5 mJ), frequency = 10 Hz, and beam diameter = 55 µm. Each optimal laser analysis lasted 2 min, encompassing 30 s to 60 s of laser sample ablation (depending on the beam length, with beam diameter = 55 µm) and 60 s of background measurement. The laser beam length was adapted to the size of the mineral phase being analyzed.

All time-resolved raw data were exported in ASCII or FIN2 format and processed offline by in-house subroutines written in VBA language for Microsoft Excel 2010^{TM}. The average gas blank signal intensities for all elements were calculated and then subtracted from the signal intensities measured during the standard and sample ablation step. A signal drift correction was applied with a linear interpolation over time by using normalized ^{151}Eu signal intensities from the bracketing standard reference materials. A two-sigma rejection test of outliers was applied to all normalized sample Eu signal intensities. The Eu concentration of each analysis were calculated from the following equations:

$$C^{i}_{SMP}(\text{norm}) = 100 \times \frac{\hat{I}^{i,SMP}_{Nx}}{\frac{\left[\hat{I}^{i,STD}_{N2} \times (N_x - N_1) + \hat{I}^{i,STD}_{N1} \times (N_2 - N_x)\right]}{(N_2 - N_1)}} \times \frac{C^{i}_{STD}}{\sum_{i=1}^{n} c^{i}_{SMP}(\text{unnorm})} \quad (4)$$

with: $C^{i}_{SMP}(\text{unnorm}) = \frac{\hat{I}^{i}_{SMP}}{\hat{I}^{i}_{STD}/C^{i}_{STD}}$

where $\hat{I}^{i}_{SMP}$, $\hat{I}^{i}_{STD}$ and C^{i}_{STD} are the signal intensity (in cps) for each of the sample-containing elemental oxides i (1 to n), the signal intensity and the elemental oxide concentration i (in % (w/w)) of elemental oxide i in NIST 610, respectively. N_1, N_2 and N_x denote the analysis numbers in the sequence.

II.4.2 LA-ICP-Q-MS

The microanalysis of Eu in the clay fraction of the spiked COx sample (R3) was performed by a UV Laser-Ablation micro sampler CETAC® Excite (193 nm) coupled with a ThermoScientific® X series II quadrupole plasma mass spectrometer, according to the laser configuration set forth by (Monnier et al., 2018). The analytical protocol involved combinations of ^{27}Al, ^{29}Si, ^{44}Ca and ^{151}Eu analyses. Ablation spots 35 μm in diameter were introduced at an 8-Hz frequency with an energy of ≈ 2 J cm^{-2}. The analysis time for each spot was 60 s, including 20 s of background measurement with the laser off and 40 s of analysis time with the laser on. The Eu concentration was calibrated against the external standard NIST 612, the internal standard of the Si value for clay minerals and the Ca value for carbonates.

II.5 Reactive transport and sorption models

All calculations were carried out using the PhreeqC code (Version 3.3) (Parkhurst and Appelo, 2013) using the Davies Equation (Davies, 1964) to account for the ionic strength correction of solutes.

Reactions occurring in the aqueous phase as well as saturation states with respect to solid phases were calculated using the thermodynamic database ThermoChimie v9b (Giffaut et al., 2014) (Grivé et al., 2015; https://www.thermochimie-tdb.com/) (Table A2).

To model Eu adsorption, two assumptions were introduced: 1) the clay fraction governs Eu retention in assuming that illite and interstratified IS were the reactive phases with IS-combined illite (50% in weight) and smectite (50% in weight) properties (Chen et al., 2014a; Grangeon et al., 2015; Tournassat et al., 2008); and 2) the additivity (Davis et al., 1998) approach is valid, whereby the models developed for the clay model phases illite and montmorillonite (smectite) can be directly applied to the COx material without considering additional reactive phases or modifying interaction parameters in the complex multi-mineral assemblage including mixed layer illite-smectite (IS). The 2-site protolysis, non-electrostatic surface complexation and cation exchange model (2 SPNE SC/CE) (Bradbury and Baeyens, 2011) was implemented for the COx clay rock. According to the 2 SPNE SC/CE model, the surface complexation phenomenon is controlled by both weak (i.e. high quantity, limited affinity) and strong (low quantity, high affinity) sites. No competitive effect was considered between Eu and other trace metals at the adsorption sites (Bradbury and Baeyens, 2011; Marques Fernandes et al., 2015). Unless otherwise indicated, calculations were performed for COx with the lower and upper clay content limits. This approach introduces the greatest error sources, while other uncertainties associated with model parameters were not considered (Table A3). Considering in the clay-rich zone the variation in clay (40-60 wt%), the variation in illite and I/S, and a percentage of 55% of smectite in I/S (Chen et al., 2014a; Gaucher et al., 2004), range of 20–44% and 9–18% for illite and montmorillonite respectively were used in the calculations.

For the percolation experiments, the 1D coupled chemical/transport model (reactive code) implemented in phreeqC was used. For the modeling step, the two filters in PEEK, with a porosity of 9.4 vol%, were taken into account, along with the length of capillary tubes at both the cell inlet and outlet. Dead volumes were estimated by simulating HTO injection through the samples (Fig. A5). Note that results indicate the absence of dilution in the HTO solution injected through the capillary loop.

The relative magnitudes of advection and dispersion are characterized by the Peclet number, as defined by:

$$P_e = \nu L/(Dp + \lambda\nu) \quad (5)$$

where L is the sample length (m), ν the pore water velocity (m s^{-1}), Dp the pore diffusion coefficient (m^2 s^{-1}), and λ the dispersivity (m). $Dp + \lambda\nu$ represents the dispersion coefficient. The Dp value was set at 1.5 10^{-11} m^2 s^{-1} (Altmann et al., 2014). Peclet numbers were estimated in the range of 2 - 4 for compact COx samples, thus indicating the predominance of the advection mode over the diffusion mode.

The column hydrodynamic characteristics required for modeling (porosity, samples dimension,….), as well as the data used for describing Eu adsorption, can be found in Tables A1-A3.

III. Results

III.1 Batch-type experiments in the COx dispersed state

Figure 3 presents the sorption isotherm of Eu on COx as well as those published for the Eu/COx system by Descostes et al. (2017) under similar conditions. The pH and alkalinity values of the supernatant were: 7.3 ± 0.1 and 2.64 ± 0.14 meq L^{-1}, respectively. Europium sorption is constant at the lowest concentration, with Rd values around (3.5 ± 0.5)×10^4 L kg^{-1}. These values are of the same order of magnitude as those given for similar experimental conditions by both García-Gutiérrez et al. (2009) (> 3.8×10^4 L kg^{-1}) and ANDRA (2005b) (≈ 5×10^4 L kg^{-1}) yet lower than that obtained by Descostes et al. (2017) (≈ 1×10^5 L kg^{-1}).

Rd values then decrease to approx. 10^4 L kg^{-1} at the highest concentration studied ($\approx 2\times10^{-7}$ mol L^{-1} for aqueous Eu concentration). Under these conditions, our data are consistent with those of Descostes et al. (2017).

The simulation results are represented by the solid lines for the lower and upper clay fraction limits. Under the experimental conditions of this study, Eu speciation in solution is dominated by carbonate complexes. Carbonate ions also appear to be important in describing the adsorption of Eu; at the lowest Eu concentrations, adsorption is controlled by the formation of two carbonate surface complexes with strong sites ($sOEu(CO_3)$ and $sOEuOHCO_3^-$, Table A2). In this range, the model overestimates our retention data by about one order of magnitude. For the highest concentrations studied, i.e. the zone where the percolation experiments were carried out, the simulation and experimental results are consistent. Under these conditions, the contribution of weak sites to retention becomes significant (≈15%).

Given this study's objective, no further work has been carried out in search of an explanation for this discrepancies observed at the lowest Eu concentrations.

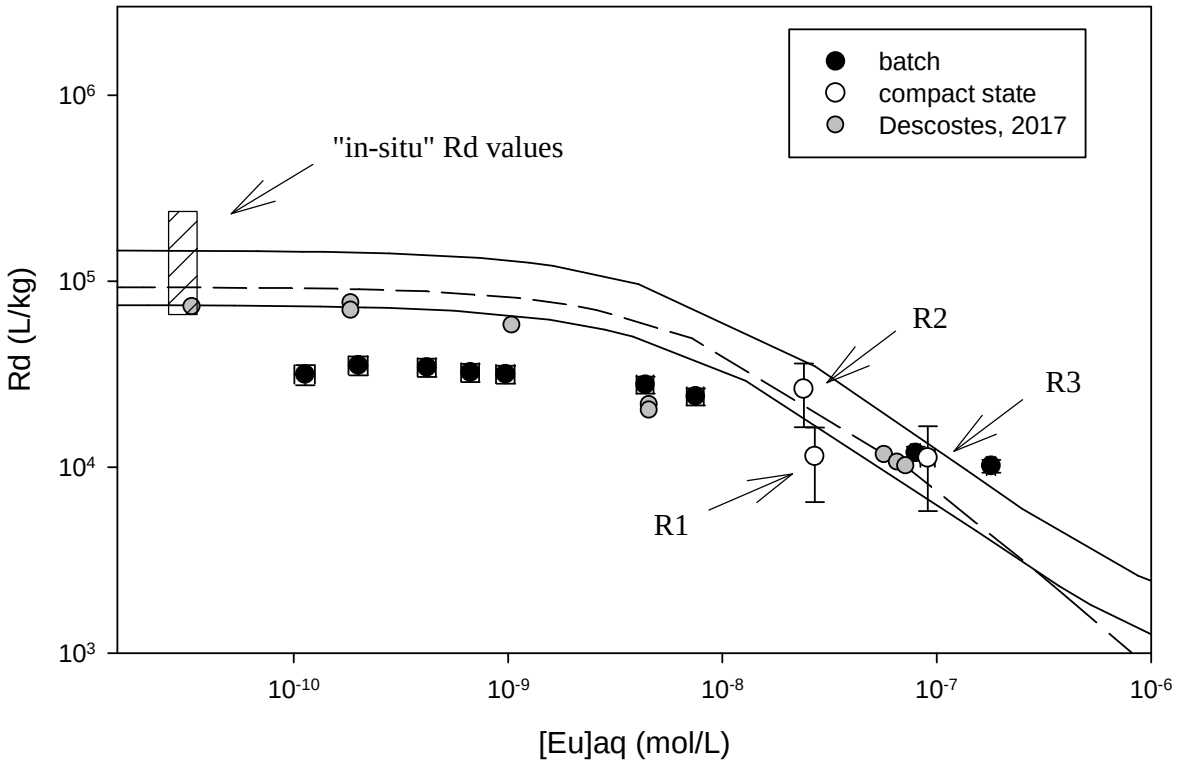

Fig. 3: Eu adsorption onto a COx sample in the presence of SPW and modeling results. (●) Batch-type experiments; (O) Percolation experiments in the compact state (R1, R2 and R3). (▲) Data from Descostes et al. (2017). Solid lines depict simulations performed for the lower and upper clay fraction limits. The dashed line represents the contribution of the two carbonate surface complexes (sOEu(CO_3) and sOEuOHCO_3^-) to the overall retention for the mean COx clay fraction. Simulation details are given in Tables A2 and A3.

III.2 Naturally-occurring Eu

The two analytical approaches (the direct analysis on the solid vs. the analysis of the solution, after digestion) yield similar values, i.e. an Eu concentration of 0.9 ± 0.2 µg g^{-1}. As expected, Eu is present at trace levels in the clay formation; to the best of our knowledge, this is the first reported value for Eu.

The various constituent mineral phases (i.e. clay, calcite, pyrite) were analyzed by means of LA-HR-ICP-MS in order to assess the distribution of naturally-occurring Eu in the COx. These mineral phases were chosen for their recognized ability to trap metals though various retention

processes (Descostes et al., 2017); results are provided in Figure 4. The mass balance calculations performed from the direct analyses carried out on individual phases did appear to be consistent, given the uncertainties present, with the total quantity of Eu in the sample. The main mineral phases with more affinity to Eu have therefore been identified.

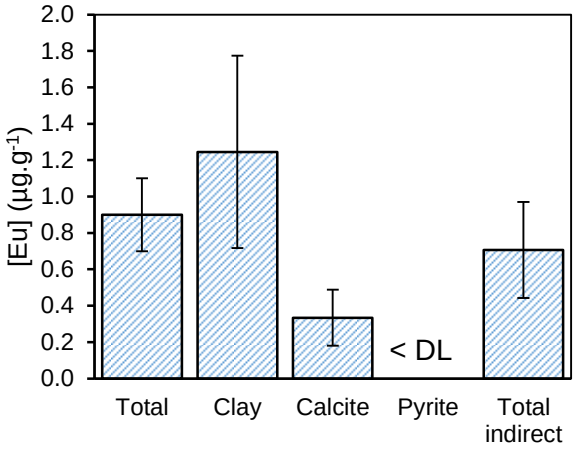

Fig. 4: Distribution of naturally-occurring Europium studied by LA-HR-ICP-MS (the number of analyses are 10, 5 and 3 for clay, calcite and pyrite, respectively). "Total indirect" corresponds to the Eu content in the COx determined by summing the Eu concentrations measured in the individual phases (normalized to their % in COx). (DL = Detection Limit)

Europium is mainly present in the clay fraction (1.2 ± 0.5 µg per g of clay fraction) and contributes to about 70% of the inventory (0.9 µg per g of COx) if the average clay content found in the COx (≈ 50 wt%) is taken into account. For calcite (≈ 25 wt%), the average Eu concentration obtained (0.33 ± 0.15 µg per g of calcite) is less than that determined in the clay phase. The contribution of calcite to average Eu concentration in the COx has been estimated at roughly 10%. No Eu was detected in the pyrite phase (i.e. < DL = 0.001 µg g^{-1}). These results indicate that the clay fraction is the main "reservoir" for Eu in the COx.

In assuming that the clay fraction controls adsorption (i.e. the starting hypothesis of the adsorption model), it is then possible to revert to Rd values as long as the concentration of Eu in the pore water remains known. A value of $(3.0 \pm 0.4)\times10^{-11}$ mol L^{-1} was experimentally measured by means of HR-ICP-MS for the GIS1002 borehole. With these concentrations in

475 water and clay fraction, a range of Rd values can be estimated from around 6.10^4 to 2.10^5 L kg^{-1}
476 (hatched area in Figure 3).

477

478 **III.3 Percolation experiments**

479 For all samples, the linearity obtained between flow rate and pressure gradient serves to validate
480 the applicability of Darcy's Law under our experimental conditions. The measured permeability
481 values varied between 3.3×10^{-13} and 4.2×10^{-13} m s^{-1} (Fig. A2); these values are in good
482 agreement with data for compact rock found in the literature (ANDRA, 2005b; Vinsot et al.,
483 2008). The COx/SPW equilibrium was checked throughout the experiment; more specifically,
484 the alkalinity and pH measured on aliquots at the reactor outlet showed values equivalent to
485 those obtained for SPW, i.e. between 2.1 and 2.4 meq L^{-1} and 7.2-7.4, respectively. The Eu
486 concentration at the outlet of all reactors remained very low and stable over time, with average
487 values below 7×10^{-11} mol L^{-1}.

488

489 *III.3.1 Europium quantification at the surface of spiked samples (R1 and R2)*

490 The analyses of Eu concentrations carried out on the surface at the inlet side of samples are
491 given in Figure 5. The ablation depth by the laser beam was estimated at about 10 µm. The
492 average Eu concentration at the surface of spiked samples equals 47 ± 19 and 95 ± 32 µg g^{-1}
493 for R1 and R2, respectively (n = 9). Europium appears to be homogeneously distributed on the
494 inlet faces even though the uncertainties associated with the derived concentrations are quite
495 high.

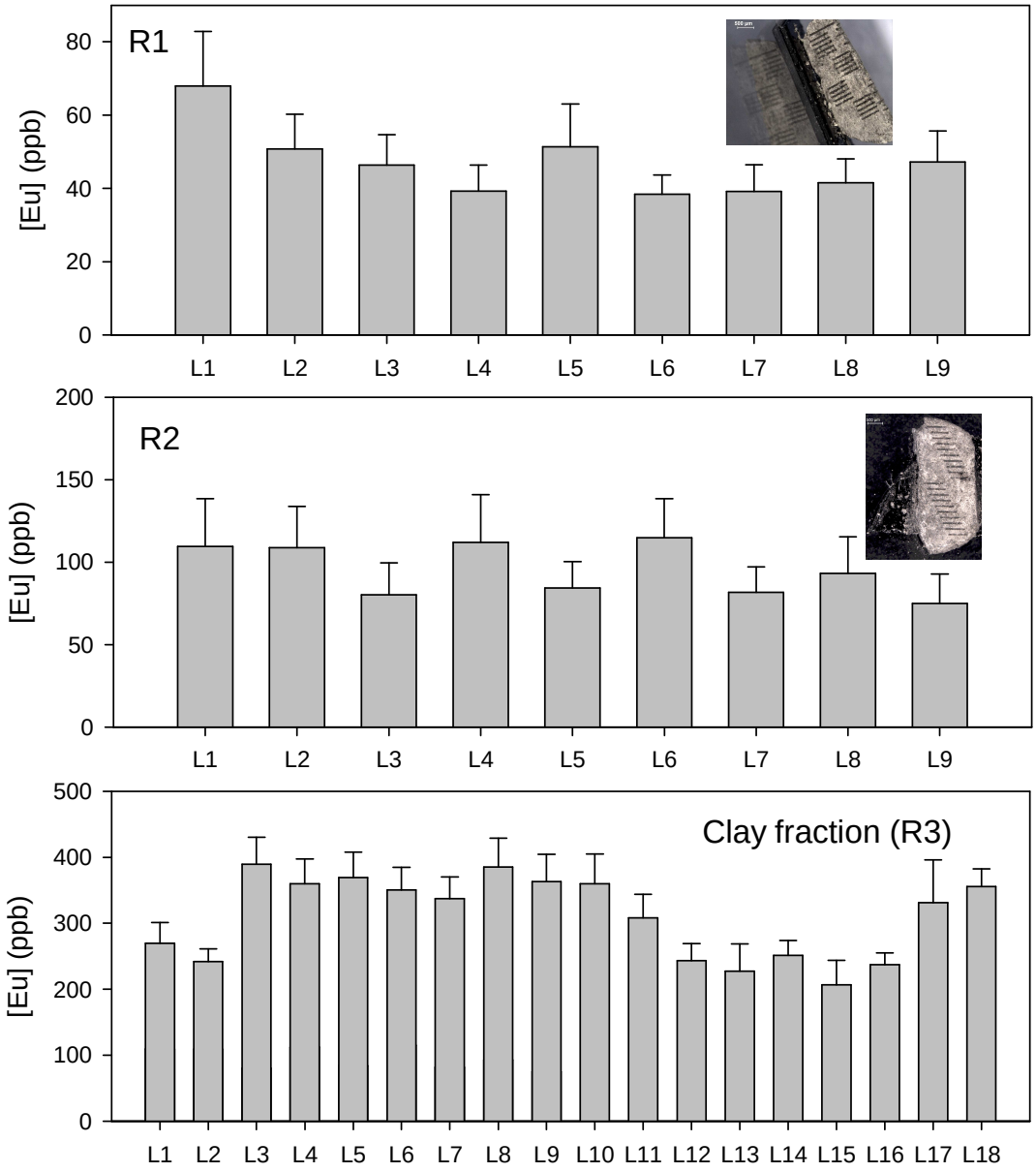

Fig. 5: Europium concentration at the surface of Eu-spiked COx samples for bulk material (R1 and R2) and clay fraction (R3). L stands for the ablation line number (average concentration over around 0.65 mm length).

During dismantling, a few drops of the aqueous solution in the immediate vicinity of the inlet surface were collected, under pressure, in order to measure the Eu concentration as close as possible to the sample surface. This analysis showed a decrease by a factor of about 3 with respect to the concentration of injected solution (8.8×10^{-8} mol L^{-1} initially), i.e. between 2.4×10^{-8} and 2.7×10^{-8} mol L^{-1}. This decrease in concentration is not easily explained. Experiments

conducted with HTO do not indicate any significant dilution resulting from the solution injection protocol (Fig. A5); moreover, the experimental set-up was designed to limit Eu adsorption on the surface of the materials used.

Regardless of the reason (e.g. possible slight adsorption of Eu on the PEEK material of the capillary loop), the measured concentrations injected into the COx sample constitute the data required to revert to the Rd values. Considering that a non-transient state was reached at the surface where pore water concentration corresponds to injected concentration, Rd values of 11,500 ± 5,000 L kg^{-1} and 26,300 ± 9,500 L kg^{-1} were obtained for R1 and R2, respectively. Although a factor of close to two lies between the values, they do agree, within the limits of uncertainty, with the predicted range of Rd values, within which the adsorption data recorded in the dispersed state all lie (open symbols in Fig. 3).

III.3.2 Eu localization at the surface of the spiked sample R3

Since no significant compaction effect was observed and given that the sorption model satisfactorily predicts the experimental retention data, Eu was expected to be adsorbed by the clay fraction. This outcome was assessed directly on the R3 sample. Note that for this reactor, unlike reactors 1 and 2, the Eu concentration measured at the reactor inlet ($9.1 \pm 0.7\ 10^{-8}$ mol L^{-1}) corresponded to the Eu concentration injected into the loop.

The areas rich in clay were previously identified by optical microscopy. Several laser ablation lines were carried out (see Fig. 5 for results). Note that the analysis of the major elements indeed confirms that the clay fraction has been appropriately targeted (Fig. A6). As expected, the Eu concentration measured in the clay matrix of the Eu-spiked COx sample ($[Eu]_{clay,R3}$) is clearly higher than that for the natural COx ($[Eu]_{clay,COx}$), i.e. 311 ± 62 µg g^{-1} vs. 1.2 ± 0.5 µg g^{-1}. In taking into account the percentage of clay in the COx ($P_{clay,COx}$), as well as the concentration of Eu injected into the compact system ($[Eu]_{injected}$), the molecular weight of Eu (MM_{Eu}) and the

fact that a non-transient state has been reached at the "interface", an Rd value can be calculated according to the following:

$$Rd = 10^{-3}\,\frac{([Eu]_{clay,R3} - [Eu]_{clay,COx})P_{clay,COx}}{MM_{Eu}[Eu]_{injected}} \quad (6)$$

The Rd value obtained (11,200 ± 5,700 L kg^{-1}) also appears to be consistent with the retention data previously determined for reactors R1 and R2 and with the values measured in the dispersed state. These results are entirely consistent with the hypothesis that clay fraction governs Eu adsorption.

III.3.3 Europium concentration along the spiked COx samples

In a final step, the Eu concentration was assessed along the samples as a function of depth for both the R1 and R2 reactors. The "percolation depth profiles" obtained are shown in Figure 6; let's note that although the profiles resemble one another, the data are rather scattered. As expected, Eu reaches its highest concentrations within the first few micrometers (< 50 μm) of the sample, even though migration was detected up to a depth of approx. 200 μm. From a depth of 200 μm and beyond, the geochemical background of Eu in COx is in fact being analyzed, i.e. approx. 0.9 μg g^{-1}.

The percolation profiles were then simulated by coupling the chemistry model applicable for the Eu concentrations investigated (solid lines in Fig. 3, see Tables A2 and A3 for the parameters) with an advective transport model (see Table A1 for detailed information). No adjustment was attempted, as this multi-parametric model lacking constraints does not output precise parameters. The simulation results (solid lines in the figure) are in good agreement with experience, provided the trends are well reproduced.

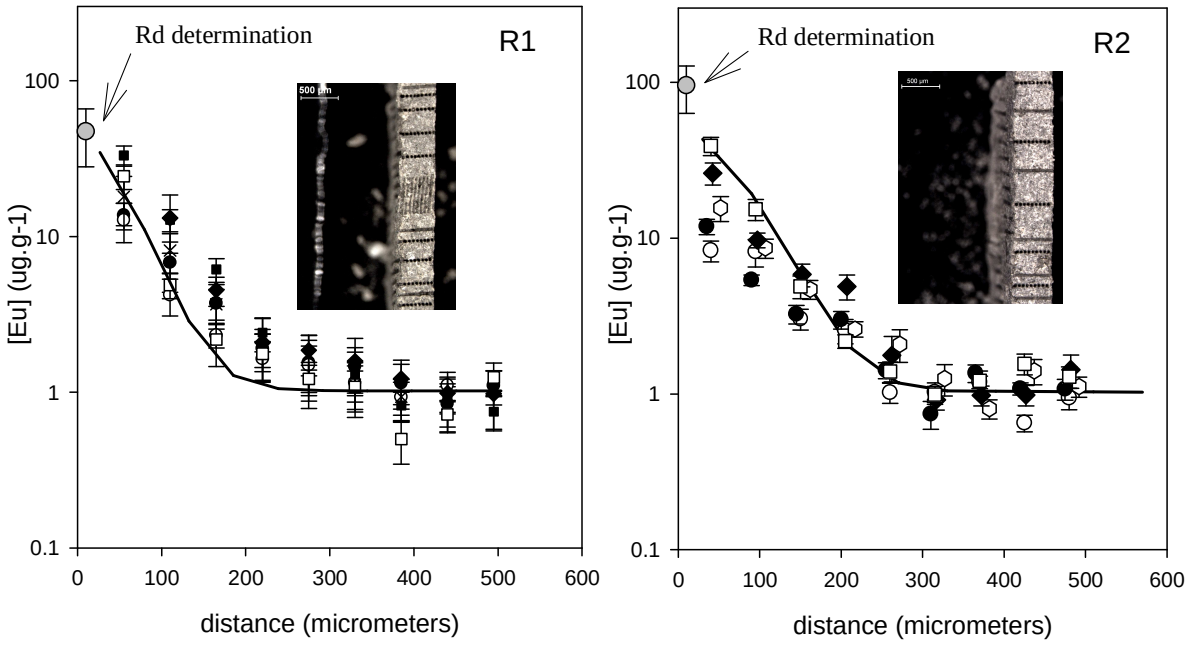

Fig. 6: Europium concentration along the COx sample for R1 (25 mL of percolated Eu-spiked SPW) and R2 (49 mL of percolated Eu-spiked SPW). The various series represent different laser ablation spot lines. The lines reflect simulations made with reactive transport model. The gray symbols correspond to the surface analysis (≈ 10 µm).

IV. Discussion

With regard to the key question raised in this work, thanks to the proposed methodology, Rd values could be proposed to describe Eu adsorption on compact COx samples. The objective of this work has been to determine these values in a non-transient state, where the thermodynamic model can be directly applied without considering the transport part. This condition is anticipated at the sample surface after a certain contact time, when the pore water concentration corresponds to that of the injected solution (dashed zone in Fig. 1).

The contact time required to reach this non-transient state at the COx pellet entry surface has not been evaluated experimentally, as this step would have required excessive experimental work given the difficulty of setting up these experiments. In this context, the simulation results prove to be quite important. As revealed by the depth profile simulation results (Fig. 6), the level of agreement between experiment and calculation is satisfactory, especially when

571 considering that no parameters have been adjusted. A more detailed examination indicates that
572 the extrapolation of simulation curves out to the surface explored by laser ablation coincides
573 with the measured Eu concentration values. Recall that these measured values are the origin of
574 the experimental Rd values, which themselves are accurately reproduced by the chemical model
575 (Fig. 3). It can thus be concluded that simulations confirm that the experimental time was
576 sufficient to achieve the desired non-transient state at the interface for R1 and R2, as proposed
577 in our strategy. Since the percolated volume is even greater for R3, the conditions are therefore
578 logically applicable to this reactor as well.

579 Europium adsorption onto COx was shown to be strong (Rd > 10^4 L kg^{-1}) at trace
580 concentrations. Similar behavior would be expected for the trivalent actinides Am and Cm, as
581 well for Pu under highly reducing conditions. Furthermore, the three Rd values obtained for the
582 compact spiked COx samples are consistent, within the experimental uncertainties, with those
583 deduced from conventional batch experiments carried out in dispersed state (black symbols in
584 Fig. 3). Similar results had already been obtained for compact COx with iodine (I) (Montavon
585 et al., 2014), cesium (Cs) (Chen et al., 2014b) and nickel (Ni) (Montavon et al., 2020), thus
586 suggesting that this trend seems *a priori* applicable to the retention of metal ions by COx clay
587 rock. The result also appears to be consistent with the recent results of Glaus et al. (2020),
588 derived from diffusion experiments vs. pH for an Eu/compacted illite system. They
589 demonstrated that adsorption models are valid for describing the equilibrium distribution of Eu
590 between aqueous solution and clay phase in the compacted state, provided an electrical double
591 layer is considered to describe the behavior of mobile species in the diffuse layer.

592 A combination of the various methods also leads to conclude that the clay fraction effectively
593 governs Eu adsorption. This finding has been indirectly confirmed by modeling the data; in
594 using a bottom-up approach along with the assumption that the clay fraction is responsible for
595 element adsorption on COx (Table A2), it was possible to explain experimental adsorption data

596 in the conditions chosen for the percolation experiments, during which both strong and weak
597 sites contribute to Eu adsorption. This finding was also validated by direct analysis on the
598 compact Eu-spiked sample (R3); the additional Eu is derived quantitatively, within
599 uncertainties, in the clay fraction. This result is in agreement with qualitative data already
600 published by Menut et al. (2006) on Eu-spiked COx samples obtained from a diffusion
601 experiment and Laser-Induced Breakdown Spectroscopy (LIBS) measurements.

602 The importance of the clay fraction in Eu retention also corroborates the results of the study
603 conducted with naturally-occurring Eu. The clay fraction represents the main reservoir, with
604 some 70% of the inventory of naturally-occurring Eu found at trace concentrations in the COx
605 ($\approx$ 0.9 mg kg^{-1}). Using this value and the natural pore water concentration of Eu, Rd values
606 ranging from 6.10^4 to 2.10^5 L kg^{-1} are determined. The domain in Rd values is consistent with
607 predictive simulations yet lies beyond the values potentially extrapolated from adsorption data
608 recorded at the trace scale (in dispersed state); the Rd values over such a range are assumed to
609 be constant ($\approx 3.5\times10^4$ L kg^{-1}). However, adsorption is not the only process leading to metal
610 retention and one shall recall that the total content of Eu in the clay rock is larger than the
611 fraction bound to the clay phases. On the other hand, only a fraction of the retained Eu is labile
612 and has to be taken into account for the evaluation of the Rd to be compared with the laboratory
613 retention experiments. Other processes leading to non-labile species, such as incorporation of
614 metals into matrices, are likely to occur, in particular for the long times characteristic of
615 sedimentary rocks (e.g. COx) (McKinley and Alexander, 1993). This outcome was recently
616 shown for the Ni/COx system (Montavon et al., 2020), whereby only $\approx$ 13% of the Ni found in
617 the rock appeared to be labile/adsorbed (and only 24% of Ni found in the clay fraction). The
618 proposed *in situ* range of Rd values ($\approx 6.10^4$ to 2.10^5 L kg^{-1}) therefore represents an upper limit,
619 which cannot be simply compared to Rd values measured in the laboratory over short time

periods. On the other hand, the deviation between prediction and experiment for equilibrium Eu concentrations below $\approx 10^{-8}$ mol L^{-1} still needs to be elucidated.

V. Conclusion

Thanks to our methodology, and the use of LA-ICP-MS, it was possible to derive Rd values for Eu on compact COx samples under non-transient conditions, i.e. without considering the transport process. Within the uncertainties present, these values are of the same order of magnitude as those derived in the dispersed state for the aqueous concentration range explored for both states (~3.10^{-8}-10^{-7} mol/L). From a mechanistic point of view, retention can be described by the reversible adsorption of Eu on the surface of clays (illite and illite/smectite) based on existing adsorption models (for equilibrium Eu concentrations above $\approx 10^{-8}$ mol L^{-1}) through carbonate surface complexes with strong sites. This finding was also shown directly by mapping on the compact spiked sample (R3); the additional Eu is found quantitatively, again within uncertainties, in the clay fraction. The magnitude of the clay fraction in Eu retention is also observed for naturally-occurring Eu, with about 70% of the inventory found in the latter. However, only a portion of this natural Eu in the clay fraction seems to be present in labile (reversible) form, thus suggesting the existence of other retention mechanisms capable of leading to metal entrapment. Further studies would be needed to assess the impact of this irreversible entrapment of Eu and of other trivalent elements in minerals for the long-term safety of radioactive waste disposal sites. Yet even when ignoring this additional margin of safety, our data clearly demonstrate the strong retention of trivalent elements on clay rock, which makes them very little mobile in the COx formation.

Acknowledgments

The authors would like to thank Andra (GL CTEC), contributors to the "Chaire stockage" unit (EDF, ORANO and Andra). This project has also received funding from the European Union's Horizon 2020 research and innovation program under grant agreement No 847593 (EURAD/FUTURE).

References

Aertsens, M., De Cannière, P., Moors, H., 2003. Modelling of silica diffusion experiments with 32 Si in Boom Clay, in: Journal of Contaminant Hydrology. Elsevier, pp. 117–129. https://doi.org/10.1016/S0169-7722(02)00140-7

Altmann, S., Aertsens, M., Appelo, T., Bruggeman, C., Gaboreau, S., Glaus, M., Jacquier, P., Kupcik, T., Maes, N., Montoya, V., Rabung, T., Robinet, J.-C., Sovoye, S., Schaefer, T., Tournassat, C., Van Laer, L., Van Loon, L., 2014. Processes of cation migration in clayrocks (CatClay) - Final Scientific Report (D1.6).

ANDRA, 2005a. Évolution Phénoménologique Du Stockage Géologique. https://www.andra.fr/cigeo/les-documents-de-reference#section-967.

ANDRA, 2005b. Dossier 2005 Argile: Tome Architecture et gestion du stockage géologique.

André, M., Malmström, M.E., Neretnieks, I., 2009. Determination of sorption properties of intact rock samples: New methods based on electromigration. J. Contam. Hydrol. 103, 71–81. https://doi.org/10.1016/j.jconhyd.2008.09.006

Bazer-Bachi, F., Tevissen, E., Descostes, M., Grenut, B., Meier, P., Simonnot, M.O., Sardin, M., 2006. Characterization of iodide retention on Callovo-Oxfordian argillites and its influence on iodide migration. Phys. Chem. Earth 31, 517–522. https://doi.org/10.1016/j.pce.2006.04.015

667 Bradbury, M.H., Baeyens, B., 2011. Predictive sorption modelling of Ni(II), Co(II), Eu(IIII),
668 Th(IV) and U(VI) on MX-80 bentonite and Opalinus Clay: A “bottom-up” approach.
669 Appl. Clay Sci. 52, 27–33. https://doi.org/10.1016/j.clay.2011.01.022

670 Chen, Z., Montavon, G., Guo, Z., Wang, X., Razafindratsima, S., Robinet, J.C., Landesman,
671 C., 2014a. Approaches to surface complexation modeling of Ni(II) on Callovo-Oxfordian
672 clayrock. Appl. Clay Sci. 101, 369–380. https://doi.org/10.1016/j.clay.2014.07.034

673 Chen, Z., Montavon, G., Ribet, S., Guo, Z., Robinet, J.C., David, K., Tournassat, C.,
674 Grambow, B., Landesman, C., 2014b. Key factors to understand in-situ behavior of Cs in
675 Callovo-Oxfordian clay-rock (France). Chem. Geol. 387, 47–58.
676 https://doi.org/10.1016/j.chemgeo.2014.08.008

677 Davies, C.W., 1964. Ion association. J. Electrochem. Soc. 111, 85C.

678 Davis, J.A., Coston, J.A., Kent, D.B., Fuller, C.C., 1998. Application of the surface
679 complexation concept to complex mineral assemblages. Environ. Sci. Technol. 32,
680 2820–2828. https://doi.org/10.1021/es980312q

681 Descostes, M., Pointeau, I., Radwan, J., Poonoosamy, J., Lacour, J.L., Menut, D., Vercouter,
682 T., Dagnelie, R.V.H., 2017. Adsorption and retarded diffusion of EuIII-EDTA− through
683 hard clay rock. J. Hydrol. 544, 125–132. https://doi.org/10.1016/j.jhydrol.2016.11.014

684 García-Gutiérrez, M., Alonso, U., Missana, T., Cormenzana, J.., Mingarro, M., Morejón, J.,
685 Gil, P., 2009. Diffusion Experiments with Opalinus and Callovo-Oxfordian Clays:
686 Laboratory, Large-Scale Experiments and Microscale Analysis by RBS. MADRID,
687 ESPAÑA.

688 Gaucher, E., Robelin, C., Matray, J.M., Négrel, G., Gros, Y., Heitz, J.F., Vinsot, A., Rebours,
689 H., Cassagnabère, A., Bouchet, A., 2004. ANDRA underground research laboratory:

690 Interpretation of the mineralogical and geochemical data acquired in the Callovian-
691 Oxfordian formation by investigative drilling. Phys. Chem. Earth 29, 55–77.
692 https://doi.org/10.1016/j.pce.2003.11.006

693 Gaucher, E.C., Tournassat, C., Pearson, F.J., Blanc, P., Crouzet, C., Lerouge, C., Altmann, S.,
694 2009. A robust model for pore-water chemistry of clayrock. Geochim. Cosmochim. Acta
695 73, 6470–6487. https://doi.org/10.1016/j.gca.2009.07.021

696 Giffaut, E., Grivé, M., Blanc, P., Vieillard, P., Colàs, E., Gailhanou, H., Gaboreau, S., Marty,
697 N., Madé, B., Duro, L., 2014. Andra thermodynamic database for performance
698 assessment: ThermoChimie. Appl. Geochemistry 49, 225–236.
699 https://doi.org/10.1016/j.apgeochem.2014.05.007

700 Glaus, M.A., Frick, S., Van Loon, L.R., 2020. A coherent approach for cation surface
701 diffusion in clay minerals and cation sorption models: Diffusion of Cs+ and Eu3+ in
702 compacted illite as case examples. Geochim. Cosmochim. Acta 274, 79–96.
703 https://doi.org/10.1016/j.gca.2020.01.054

704 Grambow, B., 2016. Geological disposal of radioactive waste in clay. Elements 12, 239–245.

705 Grangeon, S., Vinsot, A., Tournassat, C., Lerouge, C., Giffaut, E., Heck, S., Groschopf, N.,
706 Denecke, M.A., Wechner, S., Schäfer, T., 2015. The influence of natural trace element
707 distribution on the mobility of radionuclides. The exemple of nickel in a clay-rock. Appl.
708 Geochemistry 52, 155–173. https://doi.org/10.1016/j.apgeochem.2014.11.009

709 Grivé, M., Duro, L., Colàs, E., Giffaut, E., 2015. Thermodynamic data selection applied to
710 radionuclides and chemotoxic elements: An overview of the ThermoChimie-TDB. Appl.
711 Geochemistry 55, 85–94. https://doi.org/10.1016/j.apgeochem.2014.12.017

712 Hassan Loni, Y., David, K., Larrue, S., Grambow, B., Corona, C., Ribet, S., Chardon, P.,

713 Montavon, G., 2019. Uranium quantification of oak tree rings (Quercus petraea) from a
714 former uranium mining site by High Resolution Inductively Coupled Plasma Mass
715 spectrometry in Laser Ablation and Solution modes. Spectrochim. Acta - Part B At.
716 Spectrosc. 161, 105709. https://doi.org/10.1016/j.sab.2019.105709

717 Kasar, S., Kumar, S., Bajpai, R.K., Tomar, B.S., 2016. Diffusion of Na(I), Cs(I), Sr(II) and
718 Eu(III) in smectite rich natural clay. J. Environ. Radioact. 151, 218–223.
719 https://doi.org/10.1016/j.jenvrad.2015.10.012

720 Kautenburger, R., Beck, H.P., 2010. Influence of geochemical parameters on the sorption and
721 desorption behaviour of europium and gadolinium onto kaolinite. J. Environ. Monit. 12,
722 1295–1301. https://doi.org/10.1039/b914861b

723 Lerouge, C., Grangeon, S., Gaucher, E.C., Tournassat, C., Agrinier, P., Guerrot, C., Widory,
724 D., Fléhoc, C., Wille, G., Ramboz, C., Vinsot, A., Buschaert, S., 2011. Mineralogical
725 and isotopic record of biotic and abiotic diagenesis of the Callovian-Oxfordian clayey
726 formation of Bure (France). Geochim. Cosmochim. Acta 75, 2633–2663.
727 https://doi.org/10.1016/j.gca.2011.02.025

728 Lin, J., Liu, Y., Yang, Y., Hu, Z., 2016. Calibration and correction of LA-ICP-MS and LA-
729 MC-ICP-MS analyses for element contents and isotopic ratios. Solid Earth Sci. 1, 5–27.
730 https://doi.org/10.1016/j.sesci.2016.04.002

731 Liu, Y., Hu, Z., Gao, S., Günther, D., Xu, J., Gao, C., Chen, H., 2008. In situ analysis of
732 major and trace elements of anhydrous minerals by LA-ICP-MS without applying an
733 internal standard. Chem. Geol. 257, 34–43.
734 https://doi.org/10.1016/j.chemgeo.2008.08.004

735 Maes, N., Salah, S., Jacques, D., Aertsens, M., Van Gompel, M., De Cannière, P.,
736 Velitchkova, N., 2008. Retention of Cs in Boom Clay: Comparison of data from batch

737 sorption tests and diffusion experiments on intact clay cores. Phys. Chem. Earth 33,
738 S149–S155. https://doi.org/10.1016/j.pce.2008.10.002

739 Marques Fernandes, M., Vér, N., Baeyens, B., 2015. Predicting the uptake of Cs, Co, Ni, Eu,
740 Th and U on argillaceous rocks using sorption models for illite. Appl. Geochemistry 59,
741 189–199. https://doi.org/10.1016/j.apgeochem.2015.05.006

742 McKinley, I.G., Alexander, W.R., 1993. Assessment of radionuclide retardation: realistic
743 application of natural analogue studies. J. Contam. Hydrol. 13, 249–259.

744 Menut, D., Descostes, M., Meier, P., Radwan, J., Patrick, M., Poinssot, C., 2006. Europium
745 migration in Argilaceous Rocks : on the use of Micro Laser-Induced Breakdown
746 Spectroscopy (micro LIBS) as a Microanalysis Tool. Mater. Res. Soc. 932, 3–9.

747 Miller, A.W., Wang, Y., 2012. Radionuclide interaction with clays in dilute and heavily
748 compacted systems: A critical review. Environ. Sci. Technol. 46, 1981–1984.
749 https://doi.org/10.1021/es203025q

750 Molera, M., Eriksen, T., 2002. Diffusion of 22Na+, 85Sr2+, 134Cs+ and 57Co2+ in bentonite
751 clay compacted to different densities: Experiments and modeling. Radiochim. Acta 90,
752 753–760. https://doi.org/10.1524/ract.2002.90.9-11_2002.753

753 Monnier, L., Lach, P., Salvi, S., Melleton, J., Bailly, L., Béziat, D., Monnier, Y., Gouy, S.,
754 2018. Quartz trace-element composition by LA-ICP-MS as proxy for granite
755 differentiation, hydrothermal episodes, and related mineralization: The Beauvoir Granite
756 (Echassières district), France. Lithos 320–321, 355–377.
757 https://doi.org/10.1016/j.lithos.2018.09.024

758 Montavon, G., Lerouge, C., David, K., Ribet, S., Hassan-Loni, Y., Leferrec, M., Bailly, C.,
759 Robinet, J.-C., Grambow, B., 2020. Nickel Retention on Callovo-Oxfordian Clay:

760 Applicability of Existing Adsorption Models for Dilute Systems to Real Compact Rock.
761 Environ. Sci. Technol. https://doi.org/10.1021/acs.est.0c04381

762 Montavon, G., Sabatié-Gogova, A., Ribet, S., Bailly, C., Bessaguet, N., Durce, D., Giffaut, E.,
763 Landesman, C., Grambow, B., 2014. Retention of iodide by the Callovo-Oxfordian
764 formation: An experimental study. Appl. Clay Sci. 87, 142–149.
765 https://doi.org/10.1016/j.clay.2013.10.023

766 Oscarson, D.W., 1994. Surface diffusion: Is it an important transport mechanism in
767 compacted clays? Clays Clay Miner. 42, 534–543.
768 https://doi.org/10.1346/CCMN.1994.0420504

769 Parkhurst, D.L., Appelo, C.A.J., 2013. Description of input and examples for PHREEQC
770 version 3: a computer program for speciation, batch-reaction, one-dimensional transport,
771 and inverse geochemical calculations, Techniques and Methods. Reston, VA.
772 https://doi.org/10.3133/tm6A43

773 Schott, J., Acker, M., Barkleit, A., Brendler, V., Taut, S., Bernhard, G., 2012. The influence
774 of temperature and small organic ligands on the sorption of Eu(III) on Opalinus Clay.
775 Radiochim. Acta 100, 315–324. https://doi.org/10.1524/ract.2012.1921

776 Šelih, V.S., Van Elteren, J.T., 2011. Quantitative multi-element mapping of ancient glass
777 using a simple and robust LA-ICP-MS rastering procedure in combination with image
778 analysis. Anal. Bioanal. Chem. 401, 745–755. https://doi.org/10.1007/s00216-011-5119-
779 8

780 Sellin, P., Leupin, O.X., 2013. The use of clay as an engineered barrier in radioactive-waste
781 management - A review. Clays Clay Miner. 61, 477–498.
782 https://doi.org/10.1346/CCMN.2013.0610601

783 Tournassat, C., Lerouge, C., Blanc, P., Brendlé, J., Greneche, J.M., Touzelet, S., Gaucher,
784 E.C., 2008. Cation exchanged Fe(II) and Sr compared to other divalent cations (Ca, Mg)
785 in the bure Callovian-Oxfordian formation: Implications for porewater composition
786 modelling. Appl. Geochemistry 23, 641–654.
787 https://doi.org/10.1016/j.apgeochem.2007.11.002

788 Van Elteren, J.T., Tennent, N.H., Šelih, V.S., 2009. Multi-element quantification of
789 ancient/historic glasses by laser ablation inductively coupled plasma mass spectrometry
790 using sum normalization calibration. Anal. Chim. Acta 644, 1–9.
791 https://doi.org/10.1016/j.aca.2009.04.025

792 Van Loon, L.R., Baeyens, B., Bradbury, M.H., 2009. The sorption behaviour of caesium on
793 Opalinus Clay: A comparison between intact and crushed material. Appl. Geochemistry
794 24, 999–1004. https://doi.org/10.1016/j.apgeochem.2009.03.003

795 Van Loon, L.R., Baeyens, B., Bradbury, M.H., 2005. Diffusion and retention of sodium and
796 strontium in Opalinus clay: Comparison of sorption data from diffusion and batch
797 sorption measurements, and geochemical calculations. Appl. Geochemistry 20, 2351–
798 2363. https://doi.org/10.1016/j.apgeochem.2005.08.008

799 Van Loon, L.R., Glaus, M.A., 2008. Mechanical compaction of smectite clays increases ion
800 exchange selectivity for cesium. Environ. Sci. Technol. 42, 1600–1604.
801 https://doi.org/10.1021/es702487m

802 Vinsot, A., Mettler, S., Wechner, S., 2008. In situ characterization of the Callovo-Oxfordian
803 pore water composition. Phys. Chem. Earth 33.
804 https://doi.org/10.1016/j.pce.2008.10.048

805 Wang, X., Chen, Y., Wu, Y., 2004. Diffusion of Eu(III) in compacted bentonite - Effect of
806 pH, solution concentration and humic acid. Appl. Radiat. Isot. 60, 963–969.

https://doi.org/10.1016/j.apradiso.2004.01.008